VIVACE (Vortex Induced Vibration Aquatic Clean Energy): A New Concept in Generation of Clean and Renewable Energy From Fluid Flow

Michael M. Bernitsas
Ph.D.
Professor
Fellow ASME

Kamaldev Raghavan
Graduate Student, Ph.D. Candidate

Y. Ben-Simon
Graduate Student, N.A. Professional Degree

E. M. H. Garcia
Graduate Student, Ph.D. Pre-Candidate

Department of Naval Architecture and
Marine Engineering,
University of Michigan,
2600 Draper,
Ann Arbor, MI 48109-2145

Any device aiming to harness the abundant clean and renewable energy from ocean and other water resources must have high energy density, be unobtrusive, have low maintenance, be robust, meet life cycle cost targets, and have a 10–20 year life. The vortex induced vibration aquatic clean energy (VIVACE) converter—invented by Bernitsas and Raghavan, patent pending through the University of Michigan—satisfies those criteria. It converts ocean/river current hydrokinetic energy to a usable form of energy such as electricity using VIV successfully and efficiently for the first time. VIVACE is based on the idea of maximizing rather than spoiling vortex shedding and exploiting rather than suppressing VIV. It introduces optimal damping for energy conversion while maintaining VIV over a broad range of vortex shedding synchronization. VIV occurs over very broad ranges of Reynolds (Re) number. Only three transition regions suppress VIV. Thus, even from currents as slow as 0.25 m/s, VIVACE can extract energy with high power conversion ratio making ocean/river current energy a more accessible and economically viable resource. In this paper, the underlying concepts of the VIVACE converter are discussed. The designs of the physical model and laboratory prototype are presented. A mathematical model is developed, and design particulars for a wide range of application scales are calculated. Experimental measurements on the laboratory prototype are reported in the sequel paper and used here for preliminary benchmarking. [DOI: 10.1115/1.2957913]

1 Introduction

Ocean energy in the form of waves, currents, tides, and thermal and salinity gradients can provide an abundant supply of clean and renewable energy [1]. Several studies attest to the abundance of ocean energy in general [2] and more specifically to ocean current energy [1]. The vortex induced vibration aquatic clean energy (VIVACE) converter introduced in this paper converts ocean/river current energy to electricity. It was invented by Bernitsas and Raghavan and patented through the University of Michigan [3–6].

The VIVACE converter uses vortex induced vibrations (VIVs) for the first time to generate energy successfully and with high power conversion ratio from a fluid flow. VIVs normally cause tremendous damage to aero-, civil, mechanical, marine, offshore, and nuclear engineering structures. Ever since Leonardo da Vinci first observed VIV, circa 1500A.D., in the form of "Aeolian Tones," engineers have been trying to spoil vortex shedding and suppress VIV to prevent damage to equipment and structures. Furthermore, Von Karman at Cal Tech proved that the Tacoma Narrows bridge collapse in 1940 was due to VIV. This fluid-structure interaction phenomenon occurs due to the nonlinear resonance of cylinders (or spheres) through vortex shedding lock-in. VIV is also called synchronization between vortex shedding and cylinder (or sphere) oscillations. In this paper, the terms VIV, synchronization, vortex shedding lock-in, and nonlinear resonance are used alternatingly to refer to the same phenomenon.

The VIVACE converter design is based on the very simple idea of enhancing rather than spoiling vortex shedding and maximizing under significant damping rather than suppressing VIVs. None of the hundreds of known [1,7–9] or patented [9] devices, which can generate significant usable energy, are based on this concept. VIVACE is scalable and can extract energy from currents of velocities from 0.5 kn to 5 kn and above [5]. It is a robust system in the sense of low sensitivity to environmental conditions because vortex shedding synchronization occurs over a broad and continuous range of frequencies, not just at natural frequencies as in linear resonance. For stationary cylinders, the Karman street (stream of generated vortices) occurs over very broad ranges of Reynolds (Re) number. Only in two transition regions, VIV is suppressed. Consequently, VIV may occur over the same Reynolds number ranges.

In this paper, a brief overview of literature relevant to ocean energy conversion, the VIVACE converter, and vortex induced vibrations is presented. The challenge of designing and operating an ocean energy converter is defined in Sec. 2. The VIVACE converter is introduced in Sec. 3 by discussing the basic underlying concepts. The physical, laboratory, and mathematical models of VIVACE are presented in Sec. 4. Applications from gigascale to microscale are discussed as the principles of scaling are explained in Sec. 5. Preliminary benchmarking is performed based on model tests and measurements albeit difficulties in finding data for the leading wave energy conversion devices. Systematic model tests with the first three models of the VIVACE converter performed in the low-turbulence water free surface water (LTFSW) Channel of the Marine Hydrodynamics Laboratory (MHL) of the University of Michigan are presented in the sequel paper.

Contributed by the Ocean Offshore and Arctic Engineering Division of ASME for publication in the JOURNAL OF OFFSHORE MECHANICS AND ARCTIC ENGINEERING. Manuscript received January 30, 2007; final manuscript received July 10, 2007; published online September 16, 2008. Assoc. Editor: Dan Valentine. Paper presented at the 25th International Conference on Offshore Mechanics and Arctic Engineering (OMAE2006), Hamburg, Germany, June 4–9, 2006.

2 Background

Three areas of literature are relevant to this paper: ocean energy conversion, vortex induced vibrations, and the VIVACE converter. The first two are very extensive and only a limited overview follows as it relates to defining challenges in designing the VIVACE converter.

2.1 Ocean Energy Conversion. Due to public pressure, the California Energy Commission (CEC) [10] and the Department of Energy (DOE) of the United States [11] have defined general requirements, which ocean energy conversion devices must satisfy to be considered for license to operate in the United States. Those are the following: (1) have high energy density, (2) not obstruct navigation, (3) not diminish the value of expensive coastal real estate, (4) be friendly to marine life and the environment, (5) have low maintenance, (6) be robust, (7) meet life cycle cost targets, and (8) have a minimum life of 10–20 years.

The challenge of meeting all of these requirements has been the focus of more than 40 years of worldwide efforts—particularly in Europe and Japan and to a lesser extent in the United States [1,9,12]. Numerous devices have been designed and patented and several pilot devices have been launched [1,13,14]. A universally acceptable converter, however, has not yet been developed [9,12].

There are five sources of ocean energy: waves, currents, tides, thermal gradient, and salinity gradient. Some examples of how ocean energy converters fail to satisfy some of the CEC/DOE criteria are as follows.

(i) Converters based on surface oscillation, such as water column, buoy, flap, or pendulum [1,9], have high energy output only in a very narrow band of wave frequencies near resonance. At any particular location, waves are random allowing for a small window of optimal performance. In addition, waves occasionally apply extreme loads to structures.
(ii) Converters of wind or tidal current energy (turbines and watermills) can extract energy proportionally to their projected surface at an efficiency of 15–30% [7,13] and only for currents stronger that 2 m/s (~4 kn), below which they do not function efficiently [13].
(iii) Tidal energy converters require at least a 5 m head, and are very large and as obtrusive as water dams. They also require a 5–7 yr construction period and significant initial capital cost [13].
(iv) Most of the converters operate on the surface and near shore and occupy valuable coastal real estate.
(v) Converters such as watermills, turbines, or tidal dams disturb marine life.

2.2 VIVACE Converter. Even though the phenomenon of vortex induced vibrations has been known since 1500 A.D., no device has ever been built to generate efficiently and at a significant level electricity or other forms of usable energy from a fluid flow using VIV. A patent by Clark [15] was granted in 1999 based on a formula attributed to Rayleigh, which is similar to the Strouhal formula for St=0.2.

$$\mathrm{St} = \frac{f_{\mathrm{St}} \cdot D}{U} \tag{1}$$

Clark's design, however, cannot possibly work as its design and way of operation suppresses VIV in a multitude of ways. Yoshitake et al. [16] generated miniscule amounts of energy as a by-product of suppressing VIV of towering structures in airflow. The underlying concepts of VIVACE, design particulars, test results, dimensions for various scales of application, the principles of modularity and scaling, and some performance measures were revealed in Ref. [6] and are presented in Sec. 3.

2.3 Vortex Induced Vibrations. The literature on vortex induced vibrations of circular cylinders is very extensive, and new knowledge is developed continuously using experiments [17–22], field tests [22], and numerical simulations [22,23]. At this point in time, many of the aspects of VIV are understood well or the next research steps are well defined. Some new phenomena though still are being revealed as more research is conducted. A quick overview of some aspects of VIV, which pertain to the performance of the VIVACE converter, is presented next.

In its simplest form, a module of the VIVACE converter consists of a rigid circular cylinder mounted on elastic springs and connected to a power take-off (PTO) system via a transmission mechanism. Accordingly, literature related to free vibrations of elastically supported rigid cylinders; forced vibrations of such structures, with cylinders having 1 or 2 degrees of freedom [17,23–26] is relevant.

For a VIVACE module, the primary response mode is transverse to the flow. In-line oscillations of smaller magnitude are also observed in VIV and strengthen transverse oscillations [27]. As the flow velocity U increases, lock-in for a high mass ratio system is reached when the vortex formation frequency $f_{V,\mathrm{form}}$ is close enough to the body's natural frequency $f_{n,\mathrm{water}}$ as seen in Fig. 1. Lock-in or vortex synchronization occurs over a broad range of the reduced velocity factor U^* defined as

$$U^* = \frac{U}{f_{n,\mathrm{water}} \cdot D} \tag{2}$$

The mass ratio is defined as the total oscillating mass of the cylinder in VIV, including all oscillating appendages and 1/3 of the spring mass, divided by the displaced fluid mass m_d

$$m^* = \frac{m_{\mathrm{osc}}}{m_d} \tag{3}$$

where

$$m_d = \frac{\pi}{4}\rho_w D^2 L \tag{4}$$

where D is the cylinder diameter, L is the cylinder length, and ρ_w is the water density, and the rest of the symbols are defined in Table 1. That is, for high m^* values, up until lock-in occurs $f_{V,\mathrm{form}}=f_{\mathrm{St}}$. When synchronization occurs at U^* of about 6 in Fig. 1 (for $m^*=8.63$), $f_{V,\mathrm{mode}}$ appears and becomes equal to f_{cyl}, the frequency of oscillation of the cylinder. The difference between $f_{V,\mathrm{form}}$ and $f_{V,\mathrm{mode}}$ is explained later in this section under "wake patterns."

The phenomenon of lock-in or synchronization traditionally means that the ratio $f^*_{\mathrm{cyl}}=f_{\mathrm{cyl}}/f_{n,\mathrm{water}}$ remains close to unity, for high mass ratio [22,23,26]. For low mass ratio, the body oscillates at a distinctly higher frequency as seen in Fig. 1 and the range of synchronization opens up.

Experimentally, the departure of $f^*_{\mathrm{cyl}}=f_{\mathrm{cyl}}/f_{n,\mathrm{water}}$ from unity, through the lock-in regime, was shown in Ref. [22] and more recently was reported in Refs. [19,22–25]. Synchronization is defined as the "matching of the frequency of the periodic wake vortex mode with the body oscillation frequency" [19] or $f_{V,\mathrm{mode}}=f_{\mathrm{cyl}}$. Correspondingly, the fluid force frequency f_{fluid} must match the oscillation frequency, which is the definition of lock-in used by Sarpkaya [26,28]. The fluid frequency consists of a spectrum with $f_{V,\mathrm{mode}}=f_{\mathrm{cyl}}$ as the dominant frequency at lock-in. The rest of the components are explained under wake patterns.

The next important issue is the cylinder's amplitude of oscillation in VIV. In Fig. 2, Feng's minimum damping case [29] and Khalak and Williamson's case [19] are compared. In Fig. 2, it is apparent that in Feng's case [29] there are only two amplitude branches, namely, the "initial" branch and the "lower" branch [19,23] with a hysteretic transition between branches. The mass ratio m^* in Feng's case is very large because the experiments were conducted in air ($m^* \gg 250$). In the case of Khalak and Williamson, we see three branches with higher amplitudes, namely, the

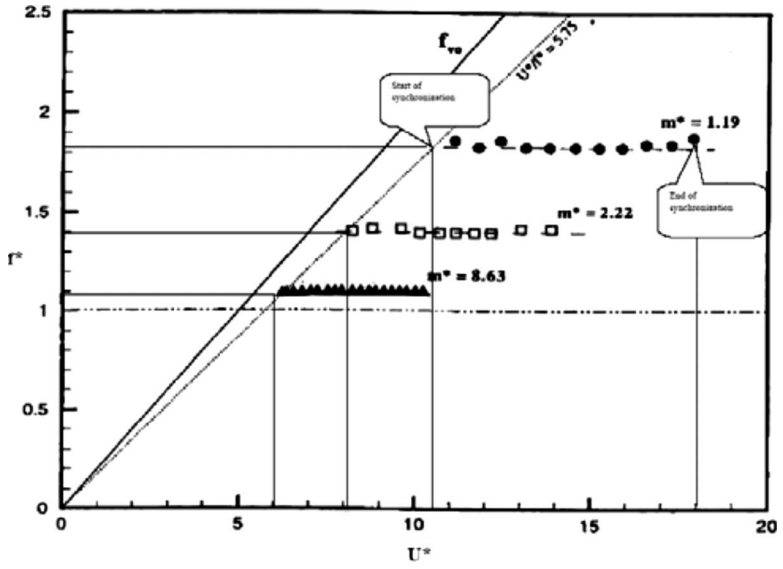

Fig. 1 Lower branch frequency response for different mass ratios versus varying U^*; reproduced from Ref. [14] here $f^*=f^*_{cyl}$

initial branch, the "upper" branch, and the lower branch. In the Khalak and Williamson case, $m^*=2.4$. There is a hysteretic transition between the initial and upper branches and intermittency between the upper and lower branches for the low mass ratio case. In recent work, however, much higher amplitudes of oscillation have been observed for higher Reynolds numbers [30,31].

In recent papers on free VIV, wake patterns that are different from the classical Karman vortex street have been reported [23–25,31]. Wake patterns that can be induced by the body motion are explained below. The wake-mode terminology was introduced by Williamson and co-workers [23–25,32]

(a) *The 2S mode*: Two single vortices shed per cylinder oscillation cycle of period T_{osc}. This is like the classical Karman street. The frequency of vortex formation $f_{V,form}$ is equal to $f_{osc}=1/T_{osc}$. The frequency of vortex wake-

Table 1 Definition of dimensional and dimensionless variables

m_{osc}	Oscillating mass including one-third of spring mass	m_d	$\frac{\pi}{4}\rho_w D^2 L$	c_{system}	From damping test with transmission disconnected
m^*	m_{osc}/m_d	m_a	$C_a m_d$	c_{tra}	From damping tests with transmission connected minus the c_{system}
y^*	y/D	y^*_{max}	y_{max}/D	c_{total}	$=c_{system}+c_{tra}+c_{gen}+c_{harn}$
y^*_{rms}	y_{rms}/D	$f_{n,water}$	$\frac{1}{2\pi}\sqrt{\frac{k}{(m+m_a)}}$	c_{gen}	From damping tests with transmission and generator connected minus c_{tra} minus c_{system}
f_{St}	$St\times U/D$	$f_{V,form}$	Vortex formation frequency	c_{harn}	From damping tests with transmission and generator connected minus c_{tra} minus c_{system} minus c_{gen}
f_{fluid}	Fluid force frequency	$f_{cyl}=f_{osc}$	Oscillating cylinder frequency	ζ_{index}	$\frac{c_{index}}{2\sqrt{k(m+C_a m_d)}}$
$f_{V,mode}$	Frequency of vortex mode	f^*_{index}	$f_{index}/f_{n,water}$	S_G	$2\pi^3 St^2(m^*\zeta_a)$
ω_{index}	$\frac{1}{2\pi f_{index}}=\frac{T_{index}}{2\pi}$	T_{index}	$1/f_{index}$	$c_y(t)$	$\frac{F_{transverse}\text{ in phase with velocity}}{\frac{1}{2}\rho U^2 DL}$
U^*	$\frac{U}{f_{n,water}D}$				

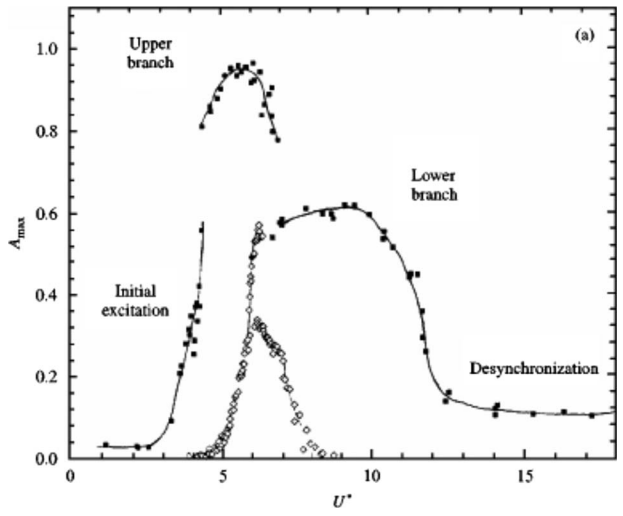

Fig. 2 Amplitude of oscillation Feng's [29] for experiments in air by Feng and experiments in water by Khalak and Williamson [19]

mode $f_{V,\text{mode}}$ is also equal to f_{osc}. Finally, the fluid forcing frequency f_{fluid} is also equal to $f_{V,\text{form}}$ and f_{osc}.

(b) *The 2P mode*: Two pairs of vortices shed per cylinder oscillation cycle of period T_{osc}. The frequency of vortex wake-mode $f_{V,\text{mode}}$ is always equal to f_{osc}. The frequency of vortex formation $f_{V,\text{form}}=2f_{V,\text{mode}}$. Finally, the fluid forcing frequency f_{fluid} has a major component equal to $f_{\text{osc}}=f_{V,\text{mode}}$ and a secondary one equal to $2f_{V,\text{mode}}$.

(c) *The P+S mode*: One vortex pair and a single vortex shed per cylinder oscillation cycle of period T_{osc}. The frequency of vortex wake-mode $f_{V,\text{mode}}$ is always equal to f_{osc}. The frequency of vortex formation $f_{V,\text{form}}=3/2f_{V,\text{mode}}$. Finally, the fluid forcing frequency f_{fluid} has a major component equal to $f_{\text{osc}}=f_{V,\text{mode}}$ and a secondary one equal to $3/2f_{V,\text{mode}}$.

(d) *The 2T mode*: Three vortex pairs shed per cylinder oscillation cycle of period T_{osc}. The frequency of vortex wake-mode $f_{V,\text{mode}}$ is always equal to f_{osc}. The frequency of vortex formation $f_{V,\text{form}}=3f_{V,\text{mode}}$. Finally, the fluid forcing frequency f_{fluid} has a major component equal to $f_{\text{osc}}=f_{V,\text{mode}}$ and a secondary one equal to $3f_{V,\text{mode}}$.

Brika and Laneville [33,34] were the first to show evidence of the $2P$ vortex wake mode in free vibration of cable due to vortex shedding [32]. The mode of vortex shedding clearly affects the amplitude of oscillation. An important issue to consider is that tests are typically performed with as small damping as possible. In our line of work, damping is not small as a rather high value induced by the PTO system is mandatory for energy extraction [35,30].

The aspect ratio (L/D) of the cylinder in VIV is an important design parameter for the operation of VIVACE. It has been studied extensively [36,37]. The aspect ratio as well as VIV have a major impact on the correlation length of the flow along the cylinder. Obviously, higher correlation length induces higher overall forces on the oscillating cylinder. Theoretically, the correlation length becomes infinite when a cylinder undergoes VIV. In practice we keep the aspect length around 20. In the Marine Hydrodynamics Laboratory of the University of Michigan, Models I, II, and III that have been tested had aspect ratios of 7.20. Models IV, V, and VI have been designed with aspect ratios of 10.29, 12.00, and 14.40, respectively. High Reynolds numbers and end plate design also have an impact on the correlation length and the maximum lift [36–38]. The wake properties depend on the aspect ratio of the cylinder [23,36].

Table 2 Pelamis data

Length	150 m
Diameter	3.5 m
Weight	380 tons
Weight with ballast	700 tons
Water depth	50 m
Life between refits	10 yr
Rated power	750 kW
Actual power (availability 40%)	300 kW

The experiments carried out for the VIVACE converter and reported in Ref. [30] are for Reynolds numbers around 10^5. It appears that higher Re results in higher lift forces and amplitudes of oscillation. Most reported amplitudes of oscillation are between 0.54 and 1.13 cylinder diameters [23]. The power VIVACE extracts from water is directly proportional to C_y the lift coefficient, as defined in Eq. (8). The amplitude of oscillation is also directly related to C_y, as shown in Eq. (30). Furthermore, C_y has an increasing trend with the Reynolds number. This probably explains the large amplitudes of oscillation that we measured with the VIVACE Models I–III. Similar results are reported in Ref. [31] for marine riser scale Reynolds numbers.

Proximity of a cylinder mounted on springs to free surface and bottom affects VIV. Even though the VIVACE converter operates fully submerged and not too close to the free surface so that it will not be obtrusive to navigation and visually unpleasant to valuable coastal real estate, tests have been conducted to ensure that the free surface impact on the laboratory tests can be assessed. Free surface would impact VIVACE in shallow water flows such as those in rivers. The free surface effect on VIV of cylinders is important because when the flow is bounded by a surface the topology of the wake and the forces on the cylinder can be significantly altered [17].

Finally, high damping is mandatory for efficient energy extraction with VIVACE. As will become obvious in the sequel paper [30], the design optimization process requires that we maintain high VIV amplitude, under high damping, over a broad range of synchronization. The peak response amplitude $y_{\max}$ varies as a function of m^* and ζ_a the damping ratio. This point is discussed, concerning especially the product of $m^*\ \zeta_a$, in Ref. [23]. In VIVACE, we maximize the generated power by adding damping to the system in the form of electrical resistance. Too much damping reduces the amplitude and may suppress VIV, as shown in Griffin's plot [23]. Increase in damping can be counteracted by decreasing the mass ratio m^* [23]. In the review papers of Williamson and Sarpkaya, it is mentioned that the product of $m^*\zeta_a$ is the parameter controlling the maximum amplitude of oscillation [23,24].

2.4 Problem Definition. Licensing of an ocean energy converter in the United States requires a design that satisfies the eight requirements listed at the beginning of Sec. 2. Model tests and measurements on the VIVACE converter provide preliminary data, which are very satisfactory. Specifically, VIVACE addresses those criteria as follows:

(1) *Energy density*. Data presented in Ref. [30] show rms value of $0.22\times\frac{1}{2}\rho U^3DL$ and a peak value of $0.31\times\frac{1}{2}\rho U^3DL$, even at this early development stage without any optimization of the design. Accordingly, the following preliminary benchmarking numbers were calculated for VIVACE using the data in Table 2: (a) energy of single module over displaced volume=0.3220 kW/m^3; (b) energy of single module over footprint volume=0.0691 kW/m^3; (c) energy of single module over weight=0.8761 kW/tons. These values appear to be two to ten times higher than the leading wave

energy converters. As will become obvious in Sec. 5, much higher energy densities are possible due to the modularity and scalability of VIVACE but at the expense of increased complexity.

(2) *Navigation*. The VIVACE converter extracts energy from currents, which run through the entire water body, not just at the water air interface. Accordingly, VIVACE whether it consists of one, a few, or thousands of oscillating cylinders remains submerged, except for the time of maintenance.

(3) *Coastal property*. A lot of ocean energy in the form of wind, waves, or currents is located along coasts. Coastal real estate is expensive and interference of any energy converter with the value of such property meets with public opposition as in the case of the wind farm off the coast of Massachusetts, a project that was cancelled in Spring 2005. VIVACE is submerged under the surface at the appropriate depth and is therefore invisible from the surface.

(4) *Marine life*. The frequency of oscillation of VIVACE is slow and can be calculated approximately by using the Strouhal vortex shedding frequency for stationary cylinders defined in Eq. (1). St is typically constant in each flow regime. St does not exist in only two transition regions where VIV is suppressed. In the laminar regime St=0.21, in the supercritical regime it varies around St=0.31, and in the postsupercritical regime it varies around St=0.46 [22]. Furthermore, the mechanism that propels cylinders in VIV transversely to the flow—that is, of accumulating and shedding large vortices—is similar to the way fishes propel in water. Fishes curve their bodies, accumulate large vortices, and then shed them by changing their body curvature [39]. Thus, it is theorized that fish will not be affected by VIVACE motion.

(5) *Maintenance*. Offshore operations are expensive. Accordingly, low maintenance cost is mandatory. The VIVACE converter has only plain cylinders exposed to the ocean environment. All other components of the power take-off system such as hydraulics, transmission, and electronics are housed in the support struts. The latter are accessible through a hydraulic telescopic hatch, which can be raised above the free surface for easy access.

(6) *Robustness*. Robustness encompasses low maintenance, minimal exposure to damage, ability to take extreme environmental loads and resume operation quickly after such events, and ability to extract energy with high efficiency over broad ranges of excitation. Currents are steady and predictable. On the contrary, waves are available about 25% of the time and vary considerably. The VIVACE converter is based on nonlinear resonance and consequently can operate in the range of synchronization over very broad ranges of current velocity variations. The low dependence of VIVACE on environmental conditions requires only slow time-scale controls. That is, we anticipate small variation of electrical damping for power extraction and slight spring stiffness adjustments to maintain VIVACE in nearly optimal operation.

(7) *Life cycle cost*. As discussed in Sec. 4, the installation cost of a 100 MW VIVACE power plant is relatively high but the estimated electricity cost is competitive due to the consistency of availability of the energy source and low maintenance.

(8) *Design life*. The VIVACE converter design is comparable to low maintenance submerged offshore facilities with template foundation. Accordingly, its design life can easily be 20 years.

3 VIVACE Converter

The VIVACE converter consists of a bluff body, which is rigid and elastically mounted or flexible, placed in a fluid flow. The body undergoes VIV and through a transmission system transmits the mechanical energy to a generator for conversion to electricity or directly to a mechanical or hydraulic form of usable energy. The subclass of the VIVACE Converter presented in this paper is that of a rigid circular cylinder mounted on linear springs and placed perpendicularly to a steady uniform current (Fig. 3). The resulting mechanical energy is transmitted via a gear-belt system to a generator and converted to electricity. First, the fundamental principles of operation of the VIVACE converter are discussed. Then, the geometry of a module and assemblies of modules are presented.

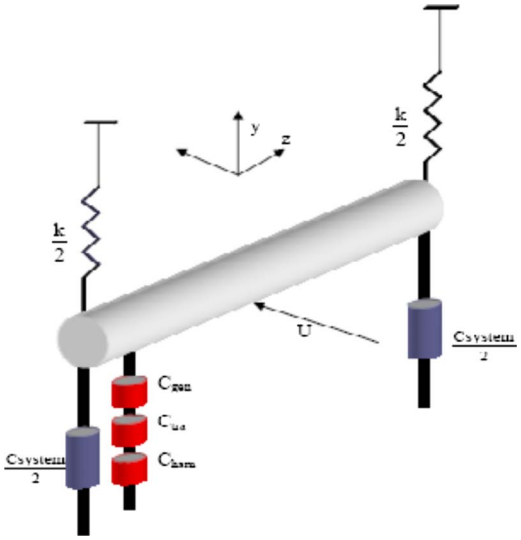

Fig. 3 Simple schematic of a VIVACE module with coordinate system

3.1 The Underlying Principles of VIVACE. The VIVACE technology is based on four principles: (a) vortex induced vibrations, (b) nonlinear resonance, (c) correlation length, and (d) energy generation. All of these concepts are interrelated.

(a) Vortex induced vibrations of a rigid circular cylinder mounted on linear springs. The phenomenon of VIV of such cylinders has been studied extensively in the past 100 yrs. Alternating vortex shedding creates asymmetry and oscillatory lift. The cylinder in VIV oscillates perpendicularly to its axis and transversely to the flow velocity (Fig. 3). Thus, the cylinder in VIV absorbs energy from the fluid. This phenomenon has been observed in several engineering disciplines: offshore (pipelines, marine risers, cables, legs of drilling, and production platforms) [22,23,28,40], nuclear (control rods in reactors), mechanical (heat exchangers), and civil (bridges, towers, and flag poles). In all occasions, systematic effort has been made to spoil vortex shedding and suppress VIV. VIVACE enhances VIV to maximize energy harnessing at high damping while maintaining a high VIV amplitude and synchronization range.

(b) Nonlinear resonance. This phenomenon is inherently related to VIV. In a broad range around the natural frequency, vortex shedding locks onto the oscillation frequency of the cylinder in VIV. The vortex shedding frequency f_{St}, as calculated for a stationary cylinder in a steady flow, ceases to exist. Frequency $f_{V,\mathrm{mode}}$ appears and becomes equal to the oscillating cylinder frequency f_{cyl}. The vortex formation frequency $f_{V,\mathrm{form}}$ depends on the wake pattern as explained in Sec. 2.3. Hence, this phenomenon is called synchronization—between vortex shedding and oscillations. Synchronization may occur (depending on the oscillating mass ratio) over a broad range around the cylinder's natural frequency in water, not just at the natural frequency. In addition, the amplitude of oscillation of the cylinder in VIV is self-limiting. Due to these last two properties, VIV is clearly a self-excited nonlinear resonance phenomenon. Ocean energy converting de-

vices based on oscillating parts (buoys, water columns, and flaps) are designed to achieve linear resonance to maximize the amplitude of oscillation. Linear resonance has a very limited bandwidth of large amplitude oscillations. The VIVACE converter is based on nonlinear resonance and enhances VIV over the entire range of nonlinear resonance while adding electrical resistance for optimal energy generation.

(c) Correlation length. In VIV, the correlation length of the flow past the cylinder is defined as the length of the cylinder along which vortices shed in phase within certain tolerance. Higher correlation length results in higher total vortex induced forces. For a circular cylinder in VIV, the correlation length is theoretically infinite. In practice, a minimum aspect ratio of 7 and a maximum of 20 are recommended. The VIVACE converter is designed with an aspect ratio in the above range. The actual choice depends on other issues tailored to the specific application and the requirements/restrictions on the values of U, m^*, m_d, and required power output. For example, the first three VIVACE models—Models I, II, and III—tested in the laboratory had an aspect ratio of 7.2. Large ocean converters will have an aspect ratio of 20.

(d) Electrical generation. The mechanical energy of a cylinder in VIV can be converted into other forms of usable energy. In VIVACE Models I–III, a belt and gear system transmits the mechanical VIV energy to a generator to convert it to electrical energy. Conversion to mechanical energy is possible, say, by using hydraulics to pump water or pressurize it for desalination. Regardless of the final form of energy, the energy converter induces mechanical damping back to the VIV system. Too much damping suppresses VIV resulting in zero harnessed energy. Too little damping will result in little harnessed energy and/or too much energy left in the VIV allowing it to reach its self-limiting value of amplitude, which in turn results in intermittent VIV. The total system damping ζ_{total}, the stiffness k of the supporting springs, and the oscillating mass m^* (Eq. (3)) can be adjusted resulting in a high degree of flexibility of the system when combined with the broad range of VIV synchronization.

3.2 Physical Model. A simple schematic of a single module of the VIVACE converter considered in this paper is depicted in Fig. 3. The elements of this module are as follows: a circular rigid cylinder of diameter D and length L, two supporting linear springs each of stiffness $k/2$, system damping c_{system}, one or more generators, generator damping c_{gen}, transmission damping c_{tra}, and the energy generating damping c_{harn}. The cylinder is placed with its axis in the z direction perpendicular to the flow velocity U, which is in the x-direction x. The cylinder oscillates in the y-direction, which is perpendicular to its axis in z and the flow velocity in x.

As discussed in Sec. 5, the VIVACE converter design is modular, scalable, and flexible in the sense of geometry and configuration. Thus, converters of various sizes can be developed by assembling modules of various sizes and properties in a variety of configurations. Figure 4 shows artist's rendition of a small array of VIVACE converter for an offshore power plant. The supporting piles, which house all the transmission and electricity generating components, are hydrodynamically faired to prevent their own VIV. The oscillating cylinders are attached by small pins to sliding bearings on a steel rod with springs and damping to provide an elastic support to achieve VIV of the cylinders.

The PTO system presently used in the VIVACE converter laboratory models consists of a gear-belt transmission system and an off-the-shelf rotary generator. Alternatives such as a hydraulic system [9] or a linear generator [9] are possible.

In the next stage of development, we will use a hydraulic system to connect multiple VIVACE modules to one generator. Direct transmission to mechanical energy through hydraulics to pump water for irrigation or raise pressure for water desalination is being studied as well.

In addition to the quantities used to define a module, for a VIVACE converter assembly, the following geometric variables need to be defined, as shown in Fig. 5: h=water depth, d=draft of the VIVACE converter assembly, t=vertical distance between centers of cylinders, and p=horizontal distance between centers of cylinders.

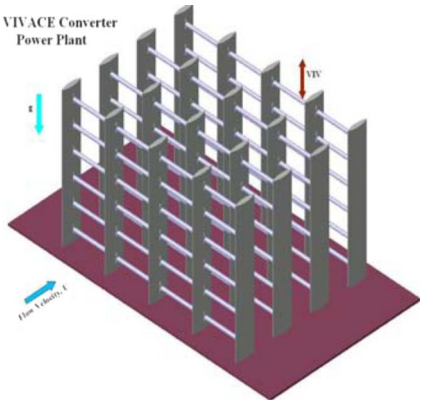

Fig. 4 Small VIVACE converter power plant

4 Modeling of VIVACE

Most of the information available in literature on free VIV (not forced oscillations) of circular cylinders falls into one of two categories: (i) laboratory tests of rigid cylinders on elastic supports at relatively low Reynolds numbers and low damping [23,26,28]. (ii) field tests of flexible cylinders at high Reynolds numbers, possibly with helical strakes or other devices to suppress VIV [22,41]. The type of tests needed for VIVACE is for a rigid cylinder mounted on elastic supports, at high Reynolds numbers, and—most important—at high damping. Accordingly, in spite of the large amount of experimental information available in literature, the specific domain of operation of VIVACE requires model tests. A series of such tests was performed on VIVACE Models I, II, and III in the LTFSW Channel of the University of Michigan and are reported in Ref. [30]. In Sec. 4.1, some information on those laboratory tests is provided as needed for this paper. Many mathematical models have been developed since the early 1900s [8] but none actually solves the boundary/initial value problem of the Navier–Stokes equations. Those models are based on numerous phenomenological assumptions and/or numerical solution techniques and consequently require extensive calibration to match measurements. A simple math model is used in Sec. 4.2 below to help understand the behavior of the VIVACE converter and verify compatibility of test measurements.

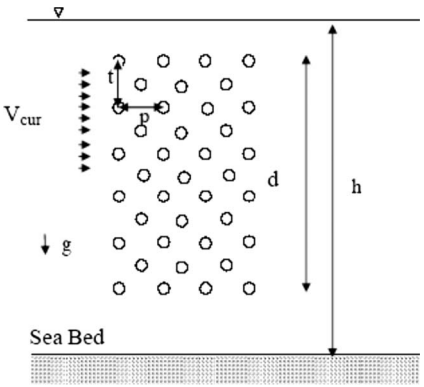

Fig. 5 Geometry, dimensions, and arrangement of cylinders in a VIVACE converter assembly

Table 3 VIVACE model particulars for test results in Fig. 6

VIVACE model particulars	
Diameter (mm)	127
Length (mm)	914.4
K of each spring (N/m)	518
Mass of the system (kg)	16.8
Mass ratio (m^*)	1.45
$f_{n,\text{water}}$ (Hz)	0.96
Velocity of current (m/s)	0.4–1.2
Reynolds number	$(0.44-1.34)\times 10^5$
Generator resistance (Ω)	7

4.1 Laboratory Model. The University of Michigan LTFSW Channel was selected for the model tests of the VIVACE converter. The LTFSW Channel provides the advantage of unlimited continuous run. The turbulence intensity normalized by the freestream velocity was reported at 0.095% [42]. The walls of the test section are made of Plexiglas, thus allowing for visualization of the flow and VIV characteristics.

Some of the properties of VIVACE Models I, II, and III are listed in Table 3. The VIVACE cylinder is made of aluminum and coated for surface smoothness and protection, as shown in Fig. 6. The aspect ratio of this cylinder is 7.274. The blockage ratio in the test section of the water channel is 14.3%. An oscillating cylinder model is suspended by two compression coil springs attached to the end plates/struts. The cylinder is constrained to vibrate freely in the transverse direction by linear bearings on shafts. There were narrow gaps of about 10 mm between the walls of water tunnel and the end plates of the model. To convert VIV into electricity, a rotary electrical generator is used. The generator is a low-rpm type typically used for wind energy conversion. A gear-belt transmission system is used to transmit the VIV linear oscillatory motion to rotational oscillatory motion of the generator shaft.

The first objective of the model tests was to confirm that the VIVACE converter can remain in nonlinear resonance throughout the design range of water current velocities, without stalling and without having to adjust the spring stiffness.

This is a measure of robustness of the VIVACE converter and is shown in Fig. 7. In Ref. [30], it is shown that the same objective can be achieved even for high damping induced by the electrical conversion load.

Our results show that Reynolds number may have a significant impact on the amplitude of VIV. Indeed, with VIVACE Model I, we measured a maximum amplitude of about $2D$ at a Reynolds number of $(0.44-1.34)\times 10^5$. Recent experiments by Exxon [31] also concluded that high amplitude oscillation is possible at high Reynolds numbers.

4.2 Mathematical Model. A simple mathematical model of the system dynamics and fluid forces is presented next. The motion of the cylinder in the y-direction (see Fig. 3) is modeled by a second order linear equation as

$$m_{\text{osc}}\ddot{y} + c_{\text{total}}\dot{y} + ky = F_{\text{fluid}}\hat{y} \tag{5}$$

where y is the direction perpendicular to the flow and the cylinder axis, m_{osc} is the oscillating system mass, which includes one-third of the spring mass, k is the spring stiffness, c_{total} is the total damping coefficient, and F_{fluid} is the force exerted by the fluid on the body in the y-direction. In this model, we separate the fluid force into viscous and inviscid components [23,24,27] as follows:

$$m_{\text{osc}}\ddot{y} + c_{\text{total}}\dot{y} + ky = F_{\text{viscous}}\hat{y} + F_{\text{inviscid}}\hat{y} \tag{6}$$

The inviscid force may be defined in terms of the inviscid added mass m_a. The added mass inclusion through a constant added mass coefficient (from potential theory) on the left hand side is still debated. This approach is based on Refs. [19,23] where the controversy on added mass of an accelerating body is addressed. The added mass is defined as "the impulse given to the fluid during an incremental change of body velocity, divided by that incremental velocity." Furthermore,

$$F_{\text{inviscid}}\hat{y} = -m_a\ddot{y} \tag{7}$$

$$F_{\text{viscous}}\hat{y} = \frac{1}{2}c_y(t)\rho U^2 DL \tag{8}$$

At this stage, we introduce m_d, the mass of the displaced fluid, which for a cylinder is $\rho_w(\pi/4)D^2L$. This reduces the equation of motion to

$$(m_{\text{osc}} + m_a)\ddot{y} + c_{\text{total}}\dot{y} + ky = \frac{2}{\pi D}c_y(t)m_d U^2 \tag{9}$$

We can nondimensionalize the above equation by introducing the dimensionless variables defined in Table 1.

Use of the natural frequency of VIVACE in water rather than in vacuum or air is necessary due to the big difference in the density of air and water. After substituting the nondimensional values into Eq. (9), the equation of motion becomes

$$(m^* + C_a)\cdot\left(\frac{\ddot{y}^*}{f_{n,\text{water}}^2} + \frac{4\pi\zeta_{\text{total}}\dot{y}^*}{f_{n,\text{water}}} + 4\pi^2 y^*\right) = \frac{2}{\pi}c_y(t)U^{*2} \tag{10}$$

When the system is in resonance, the cylinder dynamics is periodic and for certain wake structures nearly sinusoidal. Thus, VIV can be modeled using a linear oscillator model. Outside of the resonance range, the model has to be described by a nonlinear

Fig. 6 VIVACE model in the low-turbulence Free Surface Water Channel of the University of Michigan

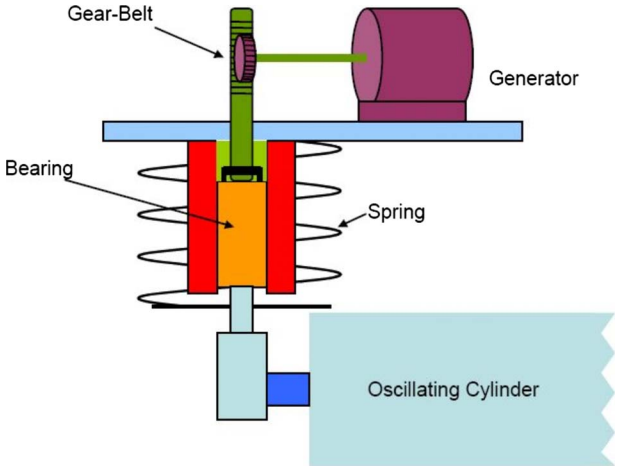

Fig. 7 Uninterrupted nonlinear resonance with no dead zones

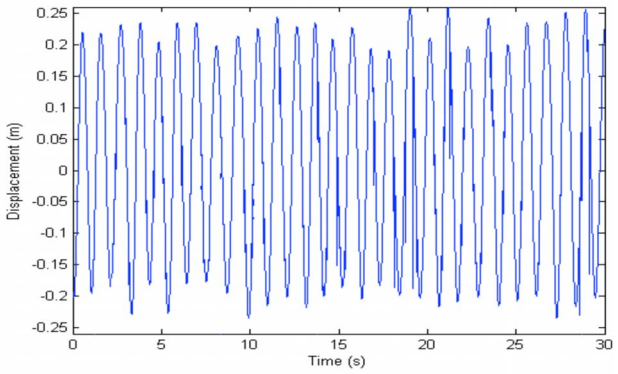

Fig. 8 Displacement versus Time for VIVACE Model I at U =0.8 m/s, D=0.127 m, for Re=0.892×10^5

model. Several wake-oscillator models have been proposed in literature [41]. To obtain a simple approximation to the resonant response without experiments, the traditional approach is to assume a sinusoidal form for the fluctuating transverse force coefficient and amplitude [38].

$$y^* = y^*_{\max} \sin(2\pi f_{\text{fluid}} t) \tag{11}$$

$$c_y(t) = C_y \sin(2\pi f_{\text{fluid}} t + \phi) \tag{12}$$

where f_{fluid} is the fluid forcing frequency, which relates to the cylinder in VIV frequency as explained in Sec. 2.3. For the ensuing analysis, f_{fluid} is assumed equal to f_{cyl}, which is the dominant fluid forcing frequency. Matching of these two quantities defines resonance. Furthermore, ϕ is the phase difference between the fluid forcing and the displacement (Fig. 8). That is, the displacement lags the forcing by an angle ϕ, which is near $\pi/2$ for linear systems at resonance. The phase angle ϕ between the fluid force and the body displacement is important in determining the energy transfer from the fluid to VIVACE. From Eqs. (10) and (12), we can deduce that $C_y \sin\phi$ has to be positive for our device to generate energy. For forced vibration, Gopalkrishnan [18] reported that for A/D=0.3, $C_y \sin\phi$ is positive for reduced velocity in the range of $5.5 < U^* < 8.0$. Also, as the amplitude of the forced oscillation increases to over 0.85, the value of $C_y \sin\phi$ becomes negative.

In free vibration experiments, $C_y \sin\phi$ can never be negative and for lower mass ratio the value of $C_y \sin\phi$ is positive for higher values of dimensionless amplitude (up to 1.13) as reported in Ref. [23]. Next, we derive expressions for the various stages of available power and for the VIVACE power conversion ratio.

Power in Fluid. The power in the flowing fluid over the projected area of the cylinder in the direction perpendicular to the flow direction can be calculated as follows. The kinetic pressure head in the fluid from Bernoulli's equation is $\frac{1}{2}\rho U^2$. The force acting over the projected area DL of the cylinder in direction X of the flow (see Fig. 3) is $\frac{1}{2}\rho U^2 DL$. Then, the power in the fluid, being the product of the acting force times the velocity in that same direction x, is

$$\text{power in the fluid} = \tfrac{1}{2}\rho U^3 DL \tag{13}$$

Equation (13) provides a fluid power for reference and nondimensionalization. It is not appropriate to use it in the denominator in efficiency calculations. A more appropriate measure of efficiency is the one used by the Department of Energy for ocean energy converters, that of energy density measured in kW/m^3. The implications of using energy density instead of efficiency is that it takes into consideration the entire space affected by the converter. For example, a ducted turbine such as the Lunar Power needs a downstream clearance of about ten duct lengths (ten duct diameters) and a vertical clearance of about one duct diameter. Furthermore, wave energy converters moored to the ocean floor obstruct use of the entire footprint volume.

Table 4 Fuel cost assumptions

Assumptions	$/MMBTU
Pulverized coal	1.25
Bituminous coal	2.75
Powder river basin coal	1.25
Uranium	0.5
Natural gas	6
Landfill gas	1.8
Capital charge	14%

Fluid Power in VIVACE. The work done by the fluid force acting on a VIVACE cylinder during a vibration cycle is obtained from the inner vector product of the force by the displacement vector $d\mathbf{x}$ integrated over 1 cycle. Therefore, the work done on the body during a cycle of oscillation of the cylinder is

$$W_{\text{VIVACE-fluid}} = \int_0^{T_{\text{cyl}}} F_{\text{fluid}} \dot{y} dt \tag{14}$$

Then, the fluid power in VIVACE is

$$P_{\text{VIVACE-fluid}} = \frac{W_{\text{VIVACE-fluid}}}{T_{\text{cyl}}} \tag{15}$$

The force exerted on the VIVACE cylinder by the fluid is given by the right hand side of Eq. (9). If we multiply the force by the instantaneous velocity, integrate the right hand side, and averaging it over the cycle period T_{osc}, we have

$$P_{\text{VIVACE-fluid}} = \frac{1}{T_{\text{cyl}}} \int_0^{T_{\text{cyl}}} \frac{2}{\pi D} c_y(t) m_d U^2 2\pi f_{\text{fluid}} y_{\max} \cos(2\pi f_{\text{fluid}} t) dt \tag{16}$$

In synchronization, we have $f_{\text{fluid}} = f_{v,\text{mode}} = f_{\text{cyl}} = 1/T_{\text{cyl}}$. Therefore,

$$\begin{aligned} P_{\text{VIVACE-fluid}} &= f_{\text{cyl}} \int_0^{1/f_{\text{cyl}}} \frac{2}{\pi D} C_y m_d U^2 2\pi f_{\text{cyl}} y_{\max} \\ &= \frac{2}{D} C_y m_d U^2 2\pi f_{\text{cyl}}^2 y_{\max} \int_0^{1/f_{\text{cyl}}} (\sin(2\pi f_{\text{cyl}} t + \phi \\ &\quad + 2\pi f_{\text{cyl}} t)\sin(2\pi f_{\text{cyl}} t + \phi)\cos(2\pi f_{\text{cyl}} t) dt \\ &\quad + \sin(2\pi f_{\text{cyl}} t + \phi - 2\pi f_{\text{cyl}} t)) dt \\ &= \frac{2}{D} C_y m_d U^2 2\pi f_{\text{cyl}}^2 y_{\max} \left(\frac{1}{f_{\text{cyl}}} \sin(\phi) + \cos(4\pi + \phi) \right. \\ &\quad \left. - \cos(\phi) \right) = \frac{2}{D} C_y m_d U^2 2\pi f_{\text{cyl}} y_{\max} \sin(\phi) \end{aligned} \tag{17}$$

Inserting the definition of m_d from Table 4, $m_d = (\pi/4)\rho D^2 L$, yields

$$P_{\text{VIVACE-fluid}} = \frac{1}{2}\rho \pi C_y U^2 f_{\text{cyl}} y_{\max} DL \sin(\phi) \tag{18}$$

Mechanical Power in VIVACE. Next, from Eq. (9), we integrate the left hand side after multiplying it by the instantaneous velocity, and we average it over the cycle period T_{cyl}. That yields the mechanical power in VIVACE.

Table 5 Estimation of an upper limit of the VIVACE power conversion ratio $\eta_{\text{UL-VIVACE}}$

	m^*	Re	C_y	Reference	U^*	$y^*_{\max}$	$\sin\phi$	$\eta_{\text{UL-VIVACE}}$
1	10.3	5000–16,000	2.83	[19,27]	5	1.18	0.1132	0.24
2	3.3	5000–16,000	4.5	[19,27]	5	1.18	0.1132	0.38
3	1.45	93,662	4.54	[27,30]	6.47	1.36	0.1132	0.37

$$P_{\text{VIVACE-mech}} = \frac{1}{T_{\text{cyl}}}\int_0^{T_{\text{cyl}}} ((m_{\text{osc}} + m_a)\ddot{y} + c_{\text{total}}\dot{y} + ky)\dot{y}dt \quad (19)$$

Only the term in phase with the velocity generates a nonzero energy term. Thus,

$$P_{\text{VIVACE-mech}} = \frac{1}{T_{\text{cyl}}}\int_0^{T_{\text{cyl}}} 4\pi(m_{\text{osc}} + m_a)\zeta_{\text{total}}\dot{y}^2 f_{n,\text{water}}dt \quad (20)$$

Using the sinusoidal expression for y from Eq. (11) into the above integral, we have

$$\begin{aligned}
&\frac{1}{T_{\text{cyl}}}\int_0^{T_{\text{cyl}}} 4\pi(m_{\text{osc}} + m_a)\zeta_{\text{total}}y_{\max}^2(\cos(2\pi f_{\text{cyl}}t))^2(2\pi f_{\text{cyl}})^2 f_{n,\text{water}}dt \\
&= \frac{1}{T_{\text{cyl}}}\int_0^{T_{\text{cyl}}} 4\pi(m_{\text{osc}} + m_a)\zeta_{\text{total}}y_{\max}^2\left(\frac{1+\cos(4\pi f_{\text{cyl}}t)}{2}\right) \\
&\quad\times(2\pi f_{\text{cyl}})^2 f_{n,\text{water}}dt \\
&= \frac{1}{T_{\text{cyl}}}(4\pi(m_{\text{osc}} + m_a)\zeta_{\text{total}}y_{\max}^2(2\pi f_{\text{cyl}})^2 f_{n,\text{water}}) \\
&\quad\times\left(\left(\frac{T_{\text{cyl}} + \sin(4\pi f_{\text{cyl}}T_{\text{cyl}})/4\pi f_{\text{cyl}}}{2}\right)\right. \\
&\quad\left.-\left(\frac{0 + \sin(4\pi f_{\text{cyl}}0)/4\pi f_{\text{cyl}}}{2}\right)\right) \\
&= 2\pi(m_{\text{osc}} + m_a)\zeta_{\text{total}}y_{\max}^2(2\pi f_{\text{cyl}})^2 f_{n,\text{water}} \\
&= 8\pi^3(m_{\text{osc}} + m_a)\zeta_{\text{total}}(y_{\max}f_{\text{cyl}})^2 f_{n,\text{water}} \quad (21)
\end{aligned}$$

Equating Fluid Power in VIVACE to Mechanical Power in VIVACE. The VIVACE fluid power in Eq. (18) and the mechanical power in Eq. (21) are equal—since they are integrals of the two sides of Eq. (9). Thus,

$$\tfrac{1}{2}\rho\pi C_y U^2 f_{\text{cyl}} y_{\max} DL\sin(\phi) = 8\pi^3(m_{\text{osc}} + m_a)\zeta_{\text{total}}(y_{\max}f_{\text{cyl}})^2 f_{n,\text{water}} \quad (22)$$

or

$$\tfrac{1}{2}\rho\pi C_y U^2 f_{\text{cyl}} y_{\max} DL\sin(\phi) = 8\pi^3\frac{\pi}{4}\rho D^2 L(m^* + C_a)\zeta_{\text{total}}(y_{\max}f_{\text{cyl}})^2 f_{n,\text{water}} \quad (23)$$

or

$$C_y U^2\sin(\phi) = 4\pi^3 D(m^* + C_a)\zeta_{\text{total}}y_{\max}f_{\text{cyl}}f_{n,\text{water}} \quad (24)$$

It is assumed that we can measure experimentally three of the four quantities C_y, $\sin(\phi)$, $y_{\max}$, and ζ_{total} and solve for the fourth quantity.

Upper Limit of VIVACE Power Conversion. The actual power converted by the VIVACE converter, $h_{\text{VIVACE}}\frac{1}{2}rU^3DL$, can be measured only during laboratory tests of the VIVACE model in the LTFSW Channel. Nevertheless, an upper limit of harnessable power, $h_{\text{UL-VIVACE}}\frac{1}{2}rU^3DL$, can be calculated either in fluid form (Eq. (18)) or in mechanical form (Eq. (21)).

$$h_{\text{UL-VIVACE}} = \frac{P_{\text{VIVACE-fluid}}}{\text{power in the fluid}} = \frac{\frac{1}{2}\rho\pi C_y U^2 f_{\text{cyl}} y_{\max} DL\sin f}{\frac{1}{2}\rho U^3 DL} \quad (25)$$

where, for a given experiment, U, D, L, ρ, and m^* are specified; f_{cyl}, $y_{\max}$, and ϕ are measured; and C_y is calculated as follows.

In Eq. (6), for $t=\frac{1}{4}T_{\text{cyl}}$ and for $t=\frac{3}{4}T_{\text{cyl}}$, the displacement is at its maximum. Thus,

$$y\left(t = \frac{1}{4}T_{\text{cyl}}\right) = y_{\max}\sin\left(2\pi f_{\text{fluid}}\frac{1}{4}T_{\text{cyl}}\right) = y_{\max} \quad (26)$$

The velocity is zero, thus eliminating the term with the unknown damping; the acceleration is at its maximum, with

$$\ddot{y}\left(t = \frac{1}{4}T_{\text{cyl}}\right) = -\omega_{\text{cyl}}^2 y_{\max}\sin\left(2\pi f_{\text{fluid}}\frac{1}{4}T_{\text{cyl}}\right) = -\omega_{\text{cyl}}^2 y_{\max} \quad (27)$$

Using the theoretical value of m_a for inviscid flow and Eqs. (7), (8), and (12), we derive the following expression from which C_y can be calculated

$$-(m_{\text{osc}} + m_a)\omega_{\text{cyl}}^2 y_{\max} + 0 + ky_{\max} = \frac{1}{2}\rho C_y U^2 DL\sin\left(\frac{\pi}{2} + f\right) \quad (28)$$

Table 5 shows some sample calculations of $\eta_{\text{UL-VIVACE}}$ based on Eq. (24) and experimental data. The first two cases use data from Ref. [19], and the third case uses data from VIVACE model tests in Ref. [29]. It should be noted that the value of C_y increases with lower mass ratio, increases with Reynolds number, and decreases with increasing damping [19]. Comparing Cases 1 and 2 to Case 3 we observe that m_{osc} decreases and Re increases both supporting higher values of C_y. Our tests, however, are performed for high damping values, which result in decreasing values for C_y. Of course this points out the need of optimizing for maximum output by trading off between $y_{\max}$ amplitude of oscillation and c_{harn}. Experimentally, the process is shown in Ref. [30].

Harnessable Energy Using VIVACE. The power that we can harness using the VIVACE converter is the power extracted by the generator, which is equal to the power VIVACE extracted from the fluid minus the power dissipated by the structural, transmission, and internal generator losses. To simplify calculations, we assume that the damping force due to the generator, which converts the mechanical energy to electrical energy, is in phase with the velocity term, and it behaves in the same way as structural and transmission damping. The total damping, as defined in Table 3 in dimensionless form, is

$$\zeta_{\text{total}} = \zeta_{\text{tra}} + \zeta_{\text{sys}} + \zeta_{\text{gen}} + \zeta_{\text{harn}} \quad (29)$$

Using Eq. (24), we have

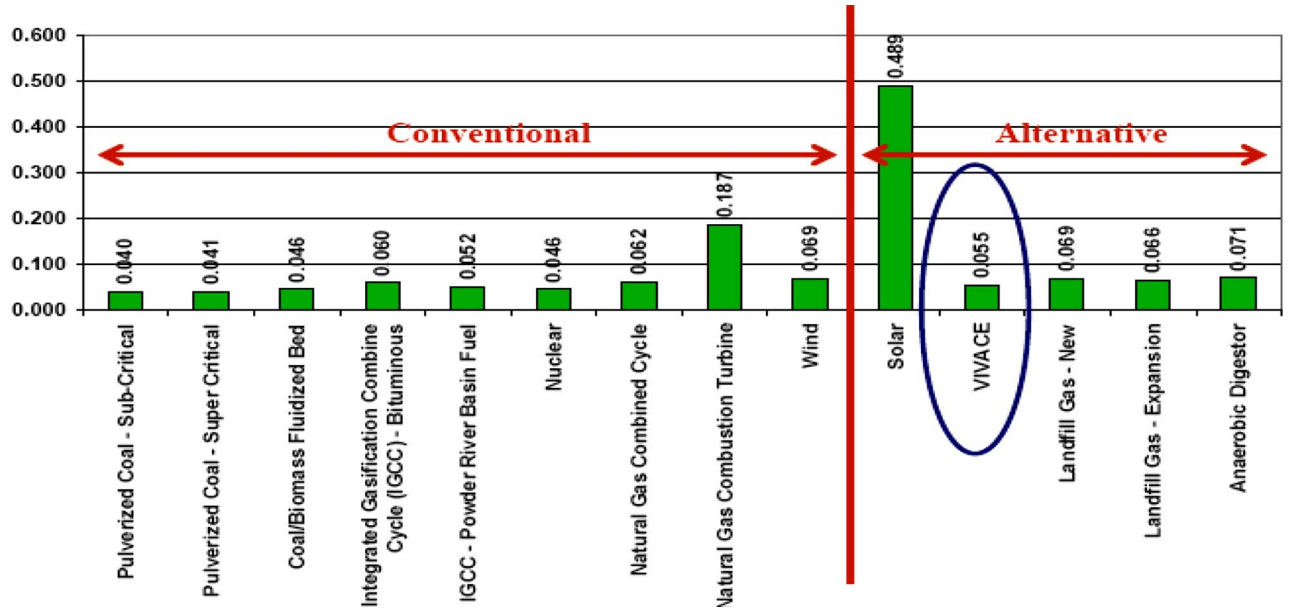

Fig. 9 Cost comparison between conventional and alternative sources of energy and the VIVACE converter [46].

$$\zeta_{\text{total}} = \frac{C_y U^2 \sin(\phi)}{4\pi^3 D(m^* + C_a) y_{\max} f_{\text{cyl}} f_{n,\text{water}}} \tag{30}$$

and in terms of the reduced velocity factor U^*, ζ_{total} can be written as

$$\zeta_{\text{total}} = \frac{C_y U^{*2} f_{n,\text{water}} \sin(\phi)}{4\pi^3 (m^* + C_a) y^*_{\max} f_{\text{cyl}}} \tag{31}$$

Combining the last two equations, we derive Eq. (32) for the damping ζ_{harn} used to harness energy

$$\zeta_{\text{harn}} = \left(\frac{C_y U^{*2} f_{n,\text{water}} \sin(\phi)}{4\pi^3 (m^* + C_a) y^*_{\max} f_{\text{cyl}}} - (\zeta_{\text{tra}} + \zeta_{\text{sys}} + \zeta_{\text{gen}}) \right) \tag{32}$$

With further manipulation, we have

$$\begin{aligned} &8\pi^3 (m + m_a) \zeta_{\text{har}} (y_{\max} f)^2 f_{n,\text{water}} \\ &\quad = \frac{\pi}{4} \rho D^2 L (2 C_y U^2 f_{\text{cyl}} y^*_{\max} \sin(\phi) - 8\pi^3 (m^* + C_a) \\ &\qquad \times (\zeta_{\text{tra}} + \zeta_{\text{sys}} + \zeta_{\text{gen}}) (y_{\max} f_{\text{cyl}})^2 f_{n,\text{water}}) \end{aligned} \tag{33}$$

which results in the final expression for the harnessed power

$$\begin{aligned} P_{\text{VIVACE-harn}} &= \frac{\pi}{4} \rho D^2 L (2 C_y U^2 f_{\text{cyl}} y^*_{\max} \sin(\phi) - 8\pi^3 (m^* + C_a) \\ &\quad \times (\zeta_{\text{tra}} + \zeta_{\text{sys}} + \zeta_{\text{gen}}) (y_{\max} f_{\text{cyl}})^2 f_{n,\text{water}}) \end{aligned} \tag{34}$$

Thus, the ratio of harnessed power to power available is

$$\eta_{\text{VIVACE}} = \frac{P_{\text{VIVACE-harn}}}{\text{power in the fluid}} = \frac{P_{\text{VIVACE-harn}}}{\frac{1}{2} \rho U^3 D L} \tag{35}$$

Even though this ratio implies efficiency, it would be controversial to define it as efficiency. As explained in Sec. 2.3, it is more appropriate to use energy density (kw/m^3) for comparison of renewable energy converters. Based on the results reported in Ref. [30], even at these early stages of development of the VIVACE converter, the power conversion ratio achieved experimentally is

$$\eta_{\text{VIVACE}} = 0.22 \tag{36}$$

for $U = 0.840$ m/s. It should be noted that the upper limit of the VIVACE converter power conversion ratio based on the model tests [28] is (see Table 5)

$$\eta_{\text{UL-VIVACE}} = 0.37 \tag{37}$$

On the basis of test measurements and evaluation of the system damping and setup, we anticipate significant increase of both numbers in future developments.

5 Design, Applications, Benchmarking

In this section, the VIVACE converter design is discussed as it may apply to various applications from small devices of a few kilowatts to offshore power plants of a gigawatt. Calculations are based on the most recent laboratory measurements of the power conversion ratio for a VIVACE converter module, which are reported in Ref. [30]. Preliminary benchmarking against other sources of energy traditional, renewable, and wave energy converters is presented as well.

5.1 Design. A VIVACE converter, generating usable energy from ocean/river currents, is modular, flexible, and scalable. Thus, it can be designed, manufactured, and installed to generate electricity in diverse applications. These three keywords as used in this paper are defined next.

(a) *Modular*. A VIVACE converter is an assembly of VIVACE modules. It may consist of a single module with a diameter of 2 cm and length of 30–40 cm to thousands of modules with cylinders of 1 m in diameter and 20 m in length.

(b) *Flexible*. The VIVACE converter is flexible in the sense that it can be designed to generate electricity from ocean/river currents in a variety of configurations for a given power output. The following design variables of a VIVACE converter and of the oscillating VIVACE cylinders allow great flexibility (see Fig. 5): number of cylinders, density of cylinders in space, cylinder dimensions (D and L), cylinder surface properties such as roughness and turbulence stimulators, cylinder relative arrangement with respect to each other (t and p), cylinder relative

Table 6 Assumptions for cost estimate of conventional energy generation [43]

Technology	Size	Capital cost	Fixed O&M	Fuel cost	Variable O&M	Availability	Cost per kW h
Conventional generation	MW	$/kW	$/kW	$/kW h	$/MW h		$/kW h
Pulverized coal—Subcritical	500	1370	42.97	0.012	1.80	85%	0.040
Pulverized coal—Supercritical	500	1437	43.60	0.011	1.70	85%	0.041
Coal/biomass fluidized bed	350	1,505	44.77	0.012	4.24	85%	0.046
Integrated gasification combine cycle (IGCC)—bituminous	550	1,647	59.52	0.025	0.95	80%	0.060
IGCC—powder river basin fuel	550	1,845	59.52	0.013	0.95	80%	0.052
Nuclear	1000	2,180	67.90	0.005	0.53	90%	0.046
Natural gas combined cycle	500	467	5.41	0.043	2.12	45%	0.062
Natural gas combustion turbine	160	375	2.12	0.063	3.71	5%	0.187

arrangement with respect to the water velocity profile, cylinder relative location in the body of water (d) from which they extract energy, cylinder oscillating mass ratio m^*, spring stiffness K, and useful damping to harness energy c_{harn}.

(c) *Scalable*. The VIVACE converter is scalable in the sense that it can be designed—based on the same four principles presented in Sec. 3—using small or large modules. As explained below, special attention has to be paid to the hydrodynamic scale defined by the Reynolds number.

Scalability and flexibility of the design of a VIVACE converter are based on the following five principles.

Principle 1. VIV of circular cylinders occurs practically over the entire range of Reynolds number (Re). VIV cannot occur in three ranges of Re, which correspond to the three ranges of no vortex shedding in a steady flow past a stationary cylinder. Hereafter we refer to these ranges as the no vortex shedding zones or dead zones.

(i) $\mathrm{Re} < 40$ corresponding to the prevortex-shedding range
(ii) $150 < \mathrm{Re} < 400$ corresponding to transition of flow from laminar to turbulent flow inside the Karman vortices
(iii) $3 \times 10^5 < \mathrm{Re} < 5 \times 10^5$ corresponding to the transition region from laminar to turbulent flow

These ranges are obtained experimentally and are valid for smooth cylinders. They are affected by various factors such as the condition of the cylinder surface, ambient flow vorticity, and fluid conditions affecting water viscosity such as salinity and temperature. Some of these factors can be modified in the design or operation state in a passive or active manner to ensure that the VIVACE cylinders remain in VIV as explained in the next principle.

Principle 2. Modifications to the basic geometry of the oscillating cylinder in a passive or active manner can be designed and built to ensure that a VIVACE cylinder can remain in VIV for the entire practical range of Reynolds numbers. Following is a nonexhaustive list of techniques, which are used to implement this principle to achieve scalability and flexibility of the VIVACE converter.

(i) *Change the cylinder diameter*. Reynolds number changes linearly proportionally with the diameter. This change is practical only when small changes in Re are sufficient to move a flow out of a dead zone.
(ii) *Introduce surface roughness*. It has a strong impact on the location of the dead zones on the Re scale. Introducing surface roughness passively is very effective when the incoming flow conditions are known a priori and do not change significantly in time.
(iii) *Introduce fixed (passive) turbulence stimulators*. Like surface roughness, turbulence stimulators have a strong impact on the location of the dead zones on the Re scale. They are very effective when the incoming flow conditions are known a priori and do not change significantly in time.
(iv) *Introduce controllable (active) turbulence stimulators*. In the unlikely case of strong variation of the incoming flow velocity in time, active control through turbulence stimulators remains the last resort.

Principle 3. For a given Reynolds number, a VIVACE cylinder can be in synchronization over broad ranges depending on the oscillating mass, the displaced fluid mass, and the stiffness of the supporting springs. The synchronization range may be very long for $m^* < 0.54$ [23]. This does not result in maximum amplitude of oscillation, which would in turn contribute to increased energy generation. The VIVACE converter aims to maximize the harnessed energy overall by identifying a broad enough range of synchronization with a high enough amplitude of oscillation discussed in Principle 4. For m^* over the critical experimental value of 0.54, the range of synchronization decreases, but the amplitude of oscillation can be affected by controlling the design variables listed in Principle 4 below.

Table 7 Assumptions for cost estimate of alternative energy generation [46]

Technology	Size	Capital cost	Fixed O&M	Fuel cost	Variable O&M	Availability	Cost per kW h
Alternative generation	MW	$/kW	$/kW	$/kW h	$/MW h		$/kW h
Wind	Unknown	1200	156.43	0.000	−18.00[a]	25%	0.069
Solar	Unknown	6000	125.14	0.000	0.00	20%	0.489
VIVACE	100	3000	70.72	0.000	0.00	90%[b]	0.055
Landfill gas—New	Unknown	1200	100.00	0.018	28.22	90%	0.069
Landfill gas—Expansion	Unknown	1000	100.00	0.018	28.22	90%	0.066
Anaerobic digestor	Unknown	2500	100.00	0.000	24.82	90%	0.071

[a]Includes tax credits $18/MW h.
[b]Accounts for availability of energy source and maintenance time.

Principle 4. For a given Reynolds number, m^* defined in Principle 3 controls the range of synchronization. The amplitude of oscillation depends on m^* as well. To maximize the power harnessed by the VIVACE converter as given by Eq. (34), the following nonexclusive list of design variables are controlled both passively and actively:

(i) the supporting spring stiffness
(ii) the oscillating mass of the cylinder plus appendages
(iii) the damping C_e induced back into the VIV system by the harnessed electrical energy
(iv) the length of each VIVACE cylinder has to be long enough to ensure low m^* but not too long to result in flexural mode excitation, which will reduce the VIV correlation length

Principle 5. The energy P_{VIV}, which a VIVACE converter can extract from the flow with power conversion ratio h_{VIVACE}, is

$$P_{\mathrm{VIVACE\text{-}harn}} = \eta_{\mathrm{VIVACE}} \tfrac{1}{2} \rho_w U^3 DL \tag{38}$$

The process of maximizing h_{VIVACE} experimentally is shown in Ref. [30].

5.2 Applications. Modularity, flexibility, and scalability of the VIVACE converter make it suitable for a wide variety of applications. A nonexhaustive list of applications is provided below classified in terms of scale of harnessed electrical power. The latter is proportional to the overall dimensions of the converter even though the dimensions of the VIVACE cylinders in VIV and their relative positions vary dramatically. The power calculated in the examples below is based on

(i) flow velocity $U=1.5$ m/s ($\approx$3 kn)
(ii) power conversion ratio, $\eta_{\mathrm{VIVACE}}=0.22$, which is the rms ratio measured in the VIVACE model tests. It should be noted that this value is conservative since the system has not been optimized in any way.
(iii) Spacing between cylinders of $p=8D$ and $t=5D$. This is greater than the required minimum of $4D$ for minimal interference between stationary cylinders [43,44]. Also it is significantly larger than the in-flow and transverse clearances of $2D$ and $1D$, respectively, for a cylinder in VIV upstream from a fixed cylinder [22]. Furthermore, it is larger than the in-flow and transverse clearances of $3D$ and $1D$, respectively, for a cylinder in VIV downstream from a fixed cylinder [22]. Furthermore, as shown in Fig. 5, cylinder rows are staggered in the flow direction and aligned in the other two directions.
(iv) The weight of the foundation and the supporting struts has been calculated based on DNV regulations for similar marine foundation templates and an additional 25% for safety.

Based on these conservative assumptions, the basic design variables of VIVACE converters for a given power output can be calculated. It should be noted that there are infinite solutions for each power plant configuration. We have selected several variables and particularly D and L in such a way that the number of cylinders is not excessive. Higher number of cylinders results in higher energy density but increased complexity. Furthermore, it is assumed that a typical household uses 1 kW [45]. This provides a measure of the size of the six scales of the VIVACE converter considered in the examples below.

5.3 Benchmarking. Two benchmarking methods are used in this section. First, VIVACE is compared to traditional and alternative energy resources based on data from Ref. [46]. The comparison results are shown in Fig. 9 in terms of \$/kW h. The assumptions behind these calculations are summarized in Tables 4, 6, and 7. Table 4 shows the fuel cost per BTU; Tables 6 and 7 show the assumptions for conventional and alternative energy generations, respectively. The assumptions behind the VIVACE converter are summarized in Table 8.

Table 8 Data regarding the 100 MW VIVACE converter used in Fig. 9

Power $P_{\mathrm{VIVACE\text{-}har}}$	100 MW
D	1 m
L	20 m
m	1880 kg
m_a	16,100 kg
m^*	1
Number of cylinders	13,094
VIVACE power conversion ratio	0.22
Calculated upper limit	0.37
V_{cur}	1.5 m/s
p	$8D$
t	$5D$
water depth h	20 m
draft d	15 m
Footprint	128 acres
Weight+foundation	148,714 tons
Footprint volume of power plant	10,359,953 m^3
kW/ton	0.6701
kW/m^3 footprint volume of power plant	0.0096

The second benchmarking is performed by comparing the VIVACE converter to leading wave energy converters. This benchmarking is much more difficult to do correctly as complete sets of consistent data are not available. The three devices selected are the Pelamis [9], the OPT buoy [8,47], and the Energetech [9] converters. The data collected about these three devices are summarized in Tables 2, 9, and 10 below. The data for the VIVACE converter are summarized in Table 11. Comparison measures are presented in Figs. 10–12.

Pelamis. It is a floating ocean wave energy converter moored to the seabed. It is designed to be used as a module of a wave farm [8,47]. It is a long cylinder with four sections and three hinges, which make it flexible to follow the free surface deformation. Hinges include a hydraulic ram system to capture the energy of the relative motion of the hinged cylindrical sections. It was designed in January 1998, and a prototype was built and deployed in May 2005. It is expected to become competitive in the year 2010. It is moored in water 50–60 m deep at a location 5–10 km off-

Table 9 OPT Power Buoy data

Length	14.63 m
Diameter	4.27 m
Water depth	30 m
Life	30 yr
Rated power	20 kW
Actual power (availability 40%)	8 kW

Table 10 Energetech oscillating water column data

Length	36 m
Width	35 m
Diameter	4.27 m
Weight	485 tons
Water depth	15 m
Life	10 yr
Rated power	500 kW
Volume of the device	18,585 m^3
Foot print volume	18,900 m^3
Actual power (availability 33%)	165 kW

Table 11 VIVACE converter: data on the small-scale converter

Length	4 m
Diameter	0.2 m
Number of cylinders	328
Weight including struts and foundation	0.1 ktons
Water depth	5 m
Volume of converter	1766 m^3
Footprint volume	1962 m^3
Life	20–30 yr
U	1.5 m/s
h_{VIVACE}	0.22
Rated power	100 kW
Actual power (availability 90%)	90 kW

shore. Some relevant data are presented in Table 2.

OPT Power Buoy. It is a floating wave energy converter moored to the sea bed. The OPT Power Buoy experiences controlled oscillations in heave [36,47]. The electric generator converts the mechanical energy in the oscillations to electricity. It is designed to be used as a part of a wave farm. Electricity is transported to land through underwater cable. It was developed in 1994 and the first tests were conducted in New Jersey in 1997. A 50 kW Power Buoy is in place in Hawaii. The company has plans to build a 10 MW wave farm in the United Kingdom. Some relevant data are presented in Table 9.

Energetech Oscillating Water Column. The Energetech OWC was first developed in Australia in 1992. The first model and testing were completed in 1997 [48]. The first full scale prototype is operating in the Port Kembla Harbor. It is placed on the sea bed or is moored at a low depth and has a parabolic wave focuser. Waves push air through a turbine, which drives an electric generator. Some relevant data are presented in Table 10.

VIVACE Ocean/River Current Energy Converter. It has been introduced in this paper, and relevant data have been presented throughout and in Refs. [3–6,30]. It was first developed in late 2003, and the first three models were completed and tested in the Marine Hydrodynamics Laboratory of the University of Michigan in 2004–2005.

Since the energy density data vary with the scale and configuration of the VIVACE converter, a design comparable in scale to the three wave energy converters above is selected from Table 12 for benchmarking. This is the 100 kW device labeled as small in Table 4. On the other hand, a single module of the megascale VIVACE in Table 12 is also comparable to the three wave energy converters considered since it generates about 6.7 kW of power. The availability of VIVACE has been estimated at 90%. The 10% down time represents maintenance and reversal time of tidal currents. Both are used in the comparison in Figs. 11 and 12. The small VIVACE converter is not used in Fig. 10 because it includes multiple modules and space between them and consequently its not comparable to single module wave energy converters. The relevant data for the small-scale (100 kW) VIVACE converter and the single module of the megascale VIVACE converter are sum-

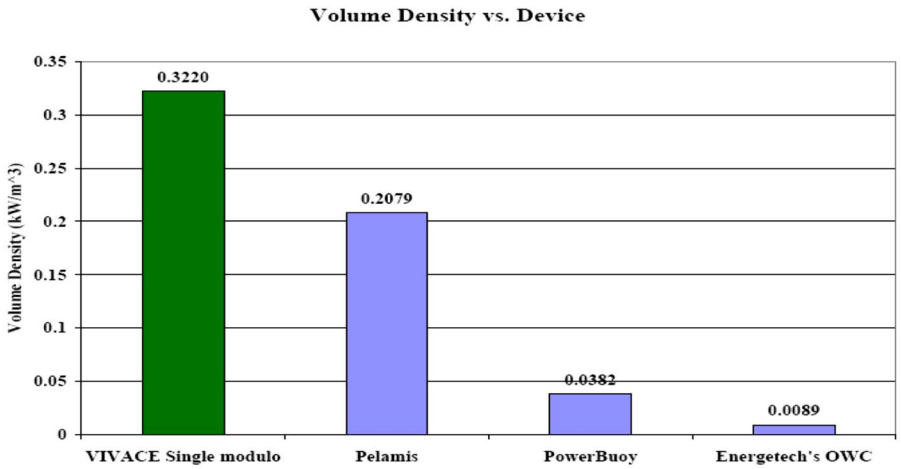

Fig. 10 Volume energy density

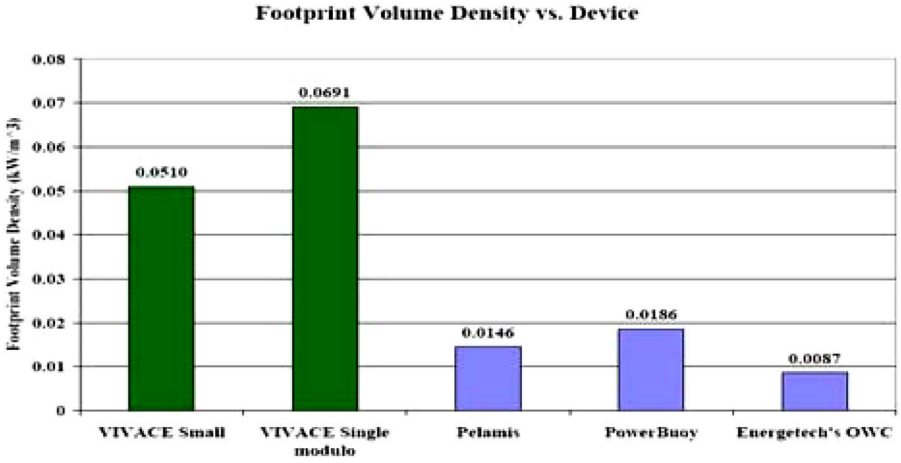

Fig. 11 Footprint volume energy density

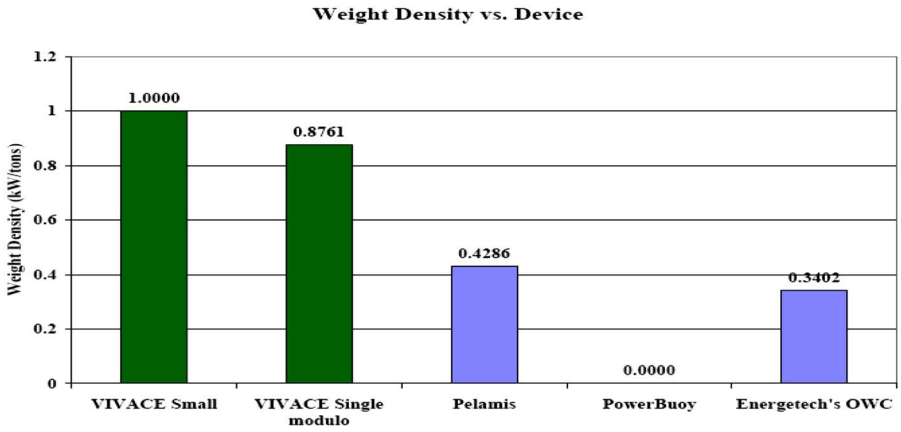

Fig. 12 Weight energy density

Table 12 Design particulars of six different scales of the VIVACE converter

Scale	Power $P_{\text{VIVACE-har}}$ (MW)	Number of cylinders	D (m)	L (m)	h (m)	S (m^2)	W (ktons)
Giga	1000	32,849	2	40	60	1,497,335	1775
Mega	100	6,570	2	20	30	258,998	159.0
Large	10	1,314	1	20	15	14,569	11.4
Medium	1	526	0.5	10	15	2428	1.1
Small	0.1	328	0.2	4	5	92	0.10
Micro	0.05	657	0.1	2	5	45	0.05

marized in Tables 11 and 13, respectively.

Data for the three wave energy converters and the two VIVACE converters are presented in Figs. 10–12. Typically the following quantities considered in comparing ocean energy converters are the following.

(a) *Volume energy density*: calculated as the actual energy generated over the volume physically occupied by a converter. The results for the devices considered are presented in Fig. 10 based on assumptions in Tables 2, 8–11, and 13.

(b) *Footprint volume energy density*: calculated as the actual energy generated over the footprint volume blocked by a converter. For example, a surface converter has a footprint at the ocean bed and the other use of the space between the footprint and the free surface is not possible. The results for the five devices considered are presented in Fig. 11.

(c) *Weight energy density*: calculated as the actual energy generated over the weight of the converter. The results for the five devices considered are presented in Fig. 12.

Table 13 VIVACE converter: data for a single module of the megascale converter

Length	20 m
Diameter	1 m
Number of cylinders	1
Weight including struts and foundation	8.675 tons
Volume of single module	23.56 m^3
Footprint volume	110 m^3
Life	20–30 yr
U	1.5 m/s
h_{VIVACE}	0.22
Rated power	7.6 kW
Actual power (availability 90%)	6.84 kW

Conclusions

A new concept for generation of clean and renewable energy from ocean/river currents has been introduced. An energy converter, nicknamed VIVACE, has been designed and tested. It extracts energy successfully by strengthening rather than spoiling vortex shedding, enhancing rather than suppressing VIV, and harnessing rather than mitigating VIV. In its simplest form, a VIVACE converter module consists of a rigid circular cylinder mounted on linear springs. Three gradually improving models—I, II, and III—have been built and tested in the Low-Turbulence Free Surface Water Channel of the University of Michigan. Based on the VIVACE design and tests, presented in Ref. [30], the following conclusions can be drawn. The VIVACE converter satisfies all requirements set by the California Energy Commission and the U.S. DOE: It is unobtrusive to navigation, the marine life, and coastal real estate; it is simple with all mechanical and electrical components sealed from the water environment; it is based on readily available offshore technology implying robustness and at least a 20 yr life; and it has high energy density. Additional advantages include consistency of current flow and its availability all year round, grid compatibility, broad range of synchronization, which allows efficient extraction of energy with minor and slow adjustment of basic design parameters such as the spring stiffness and induced damping, its ability to generate energy with high power conversion ratio even at speeds as low as 0.5 kn, and ability to extract even more energy even in the case of velocity surge to 5 kn and higher. Finally, VIVACE's scalability, modularity, and design flexibility allow for a broad range of applications.

Benchmarking with respect to conventional and alternative energy generation and wave energy converters appears very promising. Most important, there is plenty of room for improvement of the first three models built and tested. There are three areas of promising improvement at the module level: (i) optimization of the hydrodynamics of VIV including vortex shedding mode under high damping and vortex strengthening and shedding timing, (ii) optimization of the range of synchronization and the amplitude of VIV under high damping, and (iii) optimization of the power take-

off system. There are two areas of promising improvement at the power plant level: (a) optimize for the trade-off between complexity and high energy density and (b) optimize the configuration of the array of VIVACE cylinders in the three-dimensional ocean space.

Acknowledgment

This research and development project has been supported by DOE Invention and Innovations Program Grant No. DE-FG36-05GO15162 to Vortex Hydro Energy; ONR Grant No. N00014-03-1-0983 to the University of Michigan; Link Foundation through a scholarship to K R. at the University of Michigan, and by the University of Michigan Grant No. U013752/U014243.

References

[1] Pontes, M. T., and Falcão, A., 2001, "Ocean Energies: Resources and Utilization," *Proceedings of 18th WEC Congress*, Buenos Aires, Oct.
[2] World Energy Council, 2001, *Survey of Energy Resources*, 19th ed., World Energy Council, London.
[3] Bernitsas, M. M., and Raghavan, K., 2004, "Converter of Current/Tide/Wave Energy," Provisional Patent Application, U.S. Patent and Trademark Office Serial No. 60/628,252.
[4] Bernitsas, M. M., and Raghavan, K., 2005 "Supplement to the U.S. Provisional Patent Application titled 'Converter of Current, Tide, or Wave Energy'," University of Michigan Ref. No. 2973.
[5] Bernitsas, M. M., and Raghavan, K., 2005, "Fluid Motion Energy Converter," U.S. Patent Application, U.S. Patent and Trademark Office Serial No. 11/272,504.
[6] Bernitsas, M. M., and Raghavan, K., 2005, "Fluid Motion Energy Converter," International Provisional Patent Application, U.S. Patent and Trademark Office.
[7] Marine Turbines, http://www.marineturbines.com/home.htm
[8] Ocean Power Technology, http://www.oceanpowertechnologies.com
[9] WaveNet, European Wave Energy Thematic Network 2003, http://www.wave-energy.net/Library/WaveNet%20Full%20Report(11.1).pdf
[10] California Energy Commission, http://www.energy.ca.gov/
[11] Department of Energy, http://www.energy.gov/
[12] Thorpe, T. W., 1998, "An Overview of Wave Energy Technologies," Future Energy Solutions.
[13] Commission of the European Com., DGXII, 1996, "Wave Energy Project Results: The Exploitation of Tidal Marine Currents," Report EUR16683EN.
[14] International Energy Agency—Ocean Energy Systems, Status and Research and Development Priorities 2003: Wave and Marine Current Energy.
[15] Clark, R. O., 1999 "Fluid Energy Converting Method and Apparatus," U.S. Patent and Trademark Office Patent No. 4,347,036.
[16] Yoshitake, Y., Sueoka, A., Yamasaki, M., Sugimura, Y., and Ohishi, T., 2004, "Quenching of Vortex-Induced Vibrations of Towering Structure and Generation of Electricity Using Hula-Hoops," J. Sound Vib., **272**, pp. 21–38.
[17] Carberry, J., 2001, "Wake States of a Submerged Oscillating Cylinder and of a Cylinder Beneath a Free Surface," Ph.D thesis, Monash University, Australia.
[18] Gopalkrishnan, R., 1993, "Vortex Induced Forces on Oscillating Bluff Cylinders," Ph.D. thesis, Department of Ocean Engineering, MIT, Cambridge.
[19] Khalak, A., and Williamson, C. H. K., 1997, "Fluid Forces and Dynamics of a Hydroelastic Structure With Very Low Mass and Damping," J. Fluids Struct., **11**, pp. 973–982.
[20] Khalak, A., and Williamson, C. H. K., 1999, "Motions, Forces and Mode Transitions in Vortex-Induced Vibrations at Low Mass-Damping," J. Fluids Struct., **13**, pp. 813–851.
[21] Klamo, J. T., Leonard, A., and Roshko, A., 2005, "On the Maximum Amplitude for a Freely Vibrating Cylinder in Cross-Flow," J. Fluids Struct., **21**, pp. 429–434.
[22] Sumer, B. M., and Fredsoe, J., 1997, *Hydrodynamics Around Cylindrical Structures*, World Scientific, Singapore.
[23] Williamson, C. H. K., and Govardhan, R., 2004, "Vortex Induced Vibrations," Annu. Rev. Fluid Mech., **36**, pp. 413–455.
[24] Govardhan, R., and Williamson, C. H. K., 2000, "Modes of Vortex Formation and Frequency Response of a Freely Vibrating Cylinder," J. Fluid Mech., **420**, pp. 85–130.
[25] Jauvtis, N., and Williamson, C. H. K., 2003, "Vortex-Induced Vibration of a Cylinder in Two Degrees of Freedom," J. Fluids Struct., **17**, pp. 1035–1048.
[26] Sarpkaya, T., 2004, "A Critical Review of the Intrinsic Nature of Vortex Induced Vibrations," J. Fluids Struct., **19**(4), pp. 389–447.
[27] Govardhan, R., 2000, "Vortex Induced Vibration of Two and Three Dimensional Bodies," thesis, Faculty of Graduate School of Cornell University, Ithaca, NY.
[28] Sarpkaya, T., 1995, "Hydrodynamic Damping, Flow-Induced Oscillations, and Biharmonic Response," ASME J. Offshore Mech. Arct. Eng., **117**, pp. 232–238.
[29] Feng, C. C., 1968, "The Measurements of Vortex-Induced Effects in Flow Past a Stationary and Oscillating Circular and D-Section Cylinders," M.Sc thesis, University of British Columbia.
[30] Bernitsas, M. M., Ben-Simon, Y., Raghavan, K., and Garcia, E. M. H., 2006, "The VIVACE Converter: Model Tests at High Damping and Reynolds Number Around 10^5," 25th International OMAE Conference, San Diego, CA, 10–15 June 2007.
[31] Ding, J., Balasubramanian, S., Lokken, R., and Yung, T., 2004, "Lift and Damping Characteristics of Bare and Straked Cylinders at Riser Scale Reynolds Numbers," Proceedings of OTC No. 16341.
[32] Williamson, C. H. K., and Roshko, A., 1988, "Vortex Formation in the Wake of an Oscillating Cylinder," J. Fluids Struct., **2**, pp. 355–381.
[33] Brika, D., and Laneville, A., 1993, "Vortex-Induced Vibrations of a Long Flexible Circular Cylinder," J. Fluid Mech., **250**, pp. 481–508.
[34] Brika, D., and Laneville, A., 1995, "The Hysteresis and Bifurcation Phenomena in the Aeolian Vibrations of a Circular Cylinder," Proceedings, Sixth International Conference on Flow-Induced Vibration, London, United Kingdom, 10–12 April 1995.
[35] Ben Simon, Y., 2005, "Highly Damped Vortex Induced Vibrations of Circular Cylinder," Ph.D. thesis, University of Michigan, Ann Arbor.
[36] Norberg, C. 1994, "An Experimental Investigation of the Flow Around a Circular Cylinder: Influence of Aspect Ratio," J. Fluid Mech., **258**, pp. 287–316.
[37] Szepessy, S., and Bearman, P. W., 1992, "Aspect Ratio and End Plate Effects on Vortex Shedding from a Circular Cylinder," J. Fluid Mech., **234**, pp. 191–218.
[38] Bearman, P. W., 1984, "Vortex Shedding from Oscillating Bluff Bodies," Annu. Rev. Fluid Mech., **16**, pp. 195–222.
[39] Liao, J., Beal, D. N., Lauder, G. V., and Triantafyllou, M. S., 2003, "Fish Exploiting Vortices Decrease Muscle Activity," Science, **302**, pp. 1566–1569.
[40] Morison, J. R., O'Brien, M. P., Johnson, J. W., and Schaaf, S. A., 1950, "The Force Exerted by Surface Waves on Piles," Trans. AIME, **189**, pp. 149–154.
[41] Blevins, R. D., 1990, *Flow-Induced Vibration*, 2nd ed., Van Nostrand Reinhold, New York.
[42] Walker, D. T., Lyzenga, D. R., Ericson, E. A., and Lund, D. E., 1996, "Radar Backscatter and Surface Roughness Measurements for Stationary Breaking Waves," Proc. R. Soc. London, Ser. A, **452**, pp. 1953–1984.
[43] Zdravkovich, M. M., 1997, *Flow Around Circular Cylinders (Fundamentals)*, Oxford University Press, Oxford, UK, Vol. 1.
[44] Zdravkovich, M. M., 2003, *Flow Around Circular Cylinders (Applications)*, Oxford University Press, Oxford, UK, Vol. 2.
[45] Energy Information Administration (US Department of Energy) Energy Statistics, Data, and Analysis, http://www.eia.doe.gov/
[46] Michigan Public Service Commission, 2005 Capacity Needs Forum Status Report No. U-14231.
[47] Ocean Power Technology, 2001, "Testimony to the US Congress," http://epw.senate.gov/107th/tay_0530.htm
[48] U.S. Patent and Trademark Office, http://www.uspto.gov/